SEMARAK ILMU PUBLISHING

Journal of Advanced Research in Fluid Mechanics and Thermal Sciences

Journal homepage:
https://semarakilmu.com.my/journals/index.php/fluid_mechanics_thermal_sciences/index
ISSN: 2289-7879

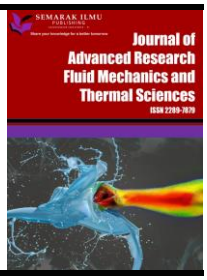

Preliminary Study on Recirculation Vortex and Turbulence Inside Ultra Low Head Pico Hydro Cross-Flow Turbine using Computational Fluid Dynamics Method

Aji Putro Prakoso[1,2], Warjito[1,*], Budiarso[1], Ahmad Fudholi[2,3]

[1] Department of Mechanical Engineering, Faculty of Engineering, Universitas Indonesia, Indonesia
[2] Research Center for Energy Conversion and Conservation, National Research and Innovation Agency (BRIN), Indonesia
[3] Solar Energy Research Institute, Universiti Kebangsaan Malaysia, Malaysia

ARTICLE INFO

Article history:
Received 20 September 2023
Received in revised form 17 December 2023
Accepted 29 December 2023
Available online 15 January 2023

Keywords:
Pico hydro; ultra low head; turbine; cross-flow; turbulence; recirculation

ABSTRACT

Cross-flow turbines (CFT) have evolved since the first investigation in 1949. After some use of computational fluid dynamics (CFD) simulations in CFT development, it is known that there might be a recirculation vortex inside the CFT. At the CFT internal flow, some significant turbulent flow occurred, which is indicated by a higher value of turbulence kinetic energy (TKE). However, the effect of the turbulence inside this turbine still evokes many questions. This study ran Several CFD simulations on three CFT blade designs. One of them has already been tested experimentally, and the others are the modifications of the first design. There are two scenarios for the simulations: run in a traditionally two-phase condition or in a submerged state to maximize the usage of the potential head. This study found that the existing configuration has a contra-directional permanent recirculation, dead area, and high turbulency spot, which induce a higher loss. Meanwhile, all those phenomena could be minimized under the modified blade condition. The modification improves multiphase CFT performance by relatively 22.2% efficiency and 16.6% relative escalation for the submerged condition. However, the expected recirculation flow found in the prior study was still not found in this study. Another modification is still needed.

1. Introduction

After being scientifically introduced in 1903, the cross-flow turbine (CFT), an invention by Hungarian engineer Donat Banki, attracted some scientists to study more about it [1]. After the published bulletin about the Banki Turbine design, manufacture, and testing by Mockmore and Merryfield [1] in 1949, this turbine experienced several evolutionary changes [2]. The first use of the Computational Fluid Dynamics (CFD) method in this turbine study since 2002 by Kaniecki [3] opened a more profound study of this turbine's flow characteristics, especially on the internal and the outflow.

* *Corresponding author.*
E-mail address: warjito@eng.ui.ac.id

https://doi.org/10.37934/arfmts.113.1.122132

Utilizing the CFD method, Choi *et al.,* [4] found that the recirculation flow inside the CFT reduces its efficiency by about 14%. The recirculation inside the CFT couldn't be seen before without the help of CFD calculation due to the phenomenon that occurred at the air phase. Adapting the National Advisory Committee for Aeronautics (NACA) airfoil to the CFT blade, Adanta *et al.,* [5] investigated the impulse characteristics of CFT. That study found that the NACA-6712 airfoil profiled blade CFT has a more significant recirculation flow, leading to this variation having a worse efficiency. These findings proved with the turbulence kinetic energy chart across the recirculation.

On the other hand, Elbatran *et al.,* [6] made some breakthrough innovations to implement CFT on ultra-low head (ULH) water flow conditions. This ULH-CFT attains about 60% efficiency at submerged conditions. Moreover, the most efficient configuration has an ample recirculation flow. Unlike the recirculation flow in the Choi *et al.,* [4] and Adanta *et al.,* [5] studies, the recirculation flow in the Elbatran *et al.,* [6] study is more centralized at only one core with the rotational direction, like the turbine rotation. Another submerged ULH-CFT configuration has also been investigated by Picone *et al.,* [7]. During the investigation, an Elbatran *et al.,* [6]-recirculation flow occurred at the turbine's internal flow. Moreover, that study found that the highest efficiency turbine has a high turbulence kinetic energy but a low turbulence eddy dissipation rate. The present study modifies an existing configured CFT blade to optimize the recirculation and turbulence flow as the proclitic of more profound studies about recirculation and turbulence flow characteristics and optimization inside the CFT.

2. Methodology

This study runs a step-by-step improvement of CFT blades to obtain a recirculation flow similar to the studies of Elbatran *et al.,* [6] and Picone *et al.,* [7]. Although those studies were done with submerged CFT configurations, this study delved into the recirculation flow in submerged and multiphase conditions. The multiphase configuration is kept to ensure the CFT initial habits as an impulse turbine runs on a multiphase condition. However, a different method of assigning head jumps between submerged and multiphase CFT is highly sensitive in a ULH condition. A multiphase CFT calculates the head as an elevation difference between the upstream reservoir water surface and the turbine's hub axis; this type of head is called a total head (H_{Tot}) in this study. In submerged conditions, the head jump is usually calculated by the elevation difference between upstream and downstream water levels since the hub is submerged under the downstream water level. This type of head jump is named as a potential head (H_{Pot}) in this study, which is equal to H_{Tot} in submerged CFT based on previous studies [7,8]. In multiphase conditions, H_{Tot} is always smaller than H_{Pot}, even until the turbine's tip blade touches the downstream water level.

The definition of the head jumps is necessary in this study to specify the value of the inlet boundary's total pressure ($p_{Tot\cdot inlet}$), which is calculated using Eq. (1). Moreover, it is also essential to select the head jumps to calculate the water potential power and efficiency. This study states the H_{Pot} is used to measure the water's potential power. This study uses two meters of H_{Pot}, with the maximum water discharge available (Q_{avail}) is 65 l/s based on the nozzle geometry. The inlet location height in the multiphase condition ($H_{inlet\cdot mp}$) is set as the vertical distance between the inlet middle point and the turbine's axis, 0.185 m. In submerged conditions, the inlet location height ($H_{inlet\cdot sm}$) is the elevation difference between the inlet midpoint and the turbine's top tip, 0.095 m. The H_{Pot}, H_{Tot}, H_{inlet}, and $p_{Tot\cdot inlet}$ for two conditions are summarized in Table 1.

$$p_{Tot\cdot inlet} = \begin{cases} (H_{Tot} - H_{inlet\cdot mp}) \text{ for multiphase condition} \\ (H_{Pot} - H_{inlet\cdot sm}) \text{ for submerged condition} \end{cases} \quad (1)$$

Using equation by Sammartano *et al.,* [2], a simple iteration method can determine the inlet velocity and the turbine's optimum rotational speed. Based on that study's experimental-result velocity coefficient and the total head jump values in this study, the optimum rotational speed for the multiphase condition is 293 RPM and 300 RPM for the submerged one. Moreover, based on the RPM prediction and the available water power, it is predicted that the specific speed of this study's turbine is about 37.5.

Table 1
Head jumps definitions for multiphase and submerged conditions

Condition	H_{Pot}	H_{Tot}	H_{inlet}
Multiphase	2 m	1.91 m	0.185 m
Submerged	2 m	2 m	0.095 m

The methodology of this study is separated into three subchapters. The first part is about the CFT design and the modification conducted, the second is about CFD simulation cases and meshing, and the last subchapter is about the CFD setups and post-processing.

2.1 The Current and Modified CFT Design

The current CFT design is the existing turbine in Fluid Mechanic Laboratories, Department of Mechanical Engineering, Faculty of Engineering Universitas Indonesia, which is the nozzle design methodology reported in a prior study [9,10]. Moreover, the significant design of the currently existing CFT is stated in Table 2. The turbine itself has been optimized previously [11]. However, the maximum efficiency that can be attained is relatively low even after the nozzle modification. This study tries to reoptimize the turbine blades since their thickness is too thick, 8 mm thickness. The modified blades use the 5-mm-thickness acrylic based on the optimal blade design in the prior study [12]. The current CFT design and the blade modification comparison can be seen in Figure 1(a) and Figure 1(b). Moreover, earlier studies agreed that the optimum blade number is between 30 and 40 [8,13]. Therefore, the second step modification changes the blade number from 20 to 30. The comparison between the 20-blade and 30-blade turbine configuration is shown in Figure 1(c).

Table 2
CFT design parameters

Parameter (Symbol) [Unit]	Value	Parameter (Symbol) [Unit]	Value
Outer diameter (D) [m]	0.180	Blade's outlet angle (β_2) [°]	90
Inner diameter (d) [m]	0.114	Blade's number (N_b)	20
O-I diam. ratio ($^{d}/_{D}$)	0.65	Nozzle's outlet angle (λ) [°]	50
Angle of attack (α) [°]	2	Nozzle initial height (S_0) [m]	0.0294
Blade's inlet angle (β_1) [°]	39		

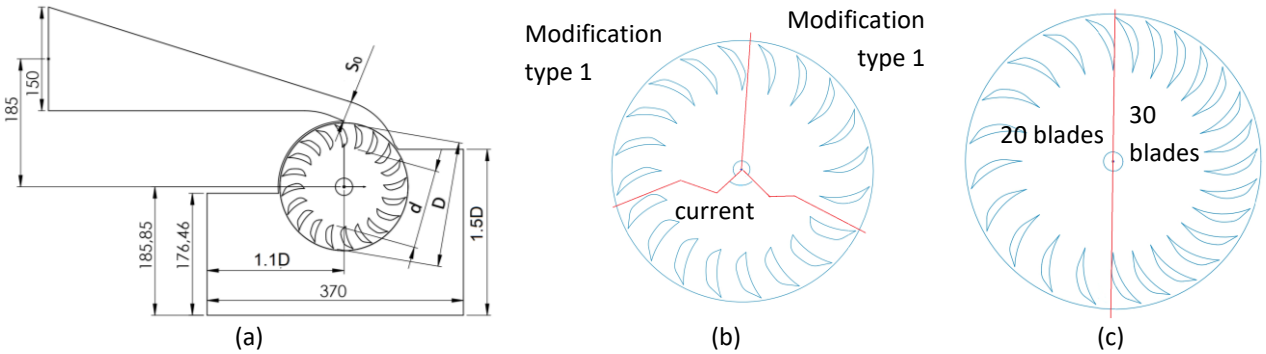

(a) (b) (c)

Fig. 1. This study's CFT design: (a) Existing design, (b) blade profile modification, (c) blade number modification

2.2 The CFD Simulation Case and Meshing

The CFD simulation in this study runs in a 2D-planar domain using ANSYS Fluent student license. The difference between a student and a commercial license is that the student license only calculates a maximum of 500 thousand mesh elements. However, as a 2D simulation, this CFD case needs less than 200 thousand mesh elements to gain an optimum simulation result. Moreover, this study used the Richardson extrapolation method to find the optimum number of mesh elements. This method uses a grid convergency index (GCI) to find the optimal mesh elements. The GCI is calculated using Eq. (2).

$$GCI_i = \frac{{}^{(f_{h=o}-f_i)}/_{f_{h=o}}}{r^p-1} \tag{2}$$

where $f_{h=o}$ is the extrapolation result by the Richardson method from the testing variable obtained from each simulation with the different number of mesh elements. The extrapolated value itself could be calculated using Eq. (3). Moreover, f_i is the value of the tested variable at the certain mesh elements number where the GCI is calculated.

$$f_{h=o} = f_1 + \frac{(f_1-f_2)}{r^p-1} \tag{3}$$

where, f_1 and f_2 is the value of the tested variable at the finest and second finest element size tested in the extrapolation process. Moreover, r is the refinement ratio used in the testing process, and p is the Richardson extrapolation convergence index, which obeys Eq. (4).

$$p = \frac{ln\left({}^{(f_2-f_3)}/_{(f_1-f_2)}\right)}{ln(r)} \tag{4}$$

The refinement ratio in Richardson extrapolation comes from the rooted ratio between a certain number of mesh elements and the finer number of mesh elements. It is recommended to keep the stable r value during several refinements. The GCI values of the Richarson extrapolation results for mesh independence testing are reported in subchapter 3.1. Moreover, the visualization of the simulation mesh distribution can be seen in Figure 2(b).

The simulation case boundaries in this simulation are displayed in Figure 2(a). The inlet of this simulation (blue line) is located at the beginning of the converging nozzle. The simulation in this study differentiates between the vertical (grey) and horizontal (green) outlet conditions. The horizontal

outlet is defined as the constant static pressure outlet and the vertical outlet is defined as the open-channel outlet to ensure the existence of the pressure variation in the vertical outlet due to the depth difference when the turbine is submerged. The rotating and static domain in the simulation is separated and connected with the interface boundary indicated by a light red circle in Figure 2(a).

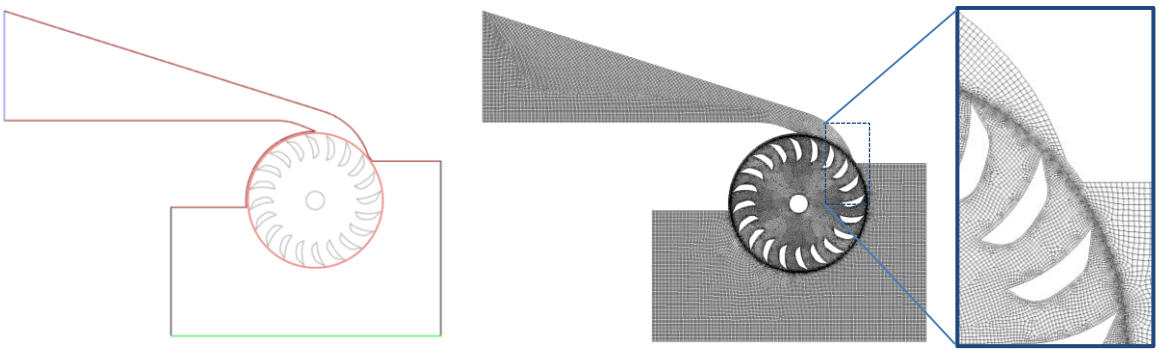

(a) (b)

Fig. 2. This study's CFD case: (a) boundaries, (b) meshing

2.3 The CFD Simulation Setups and Post-processing

This study's CFD simulations use the transient simulation for multiphase and submerged condition CFT. The energy and volume of fluid multiphase equations in this simulation are turned on. When the energy equation is turned on, the isothermal assumption is not used in the simulation. Thus, the heat transfer phenomenon is being calculated. The general energy equation that conveys the heat transfer phenomenon can be seen in Eq. (5). In multiphase flow, the energy and temperature are calculated based on mass share for each phase, as stated in Eq. (6).

$$\frac{\partial}{\partial t}(\rho E) + \nabla \cdot \left(\vec{v}(\rho E + p)\right) = \nabla \cdot \left(k_{eff}\nabla T - \sum_j h_j \vec{J}_j + \left(\bar{\bar{\tau}}_{eff} \cdot \vec{v}\right)\right) + S_h \tag{5}$$

$$E = \frac{\sum_{q=1}^{n} \alpha_q \rho_q E_q}{\sum_{q=1}^{n} \alpha_q \rho_q} \tag{6}$$

where k_{eff} is the effective thermal conductivity of the fluid, $\vec{J}_j$ is the thermal specific diffusion rate, and $\bar{\bar{\tau}}_{eff}$ is the effective turbulence shear stress. And then, the α_q and ρ_q is the volume fraction and density of any phase contained in a cell. The amount of energy (E) is calculated based on the sensible enthalpy (h) for each phase held in a numerical mesh, which can be seen in Eq. (7).

$$E = h - {}^{p}/_{\rho} + {}^{v^2}/_{2} \tag{7}$$

This study uses the 4-equations transitional SST turbulence model to solve the Boussinesq equation to solve the Reynolds averaged Navier-Stokes (RANS) equation. The recommendation of some prior studies uses the 4-equations transitional SST turbulence model [2,14,15]. The RANS equation solves the velocity and shear stress distribution due to the turbulence conditions inside the mesh. The RANS equation is stated in Eq. (8) based on ANSYS [16].

$$\frac{\partial}{\partial t}(\rho u_i) + \frac{\partial}{\partial x_j}(\rho u_i u_j) = -\frac{\partial p}{\partial x_j} + \frac{\partial}{\partial x_j}\left(\mu_t\left(\frac{\partial u_i}{\partial x_j} + \frac{\partial u_j}{\partial x_i} - {}^{2}/_{3}\,\delta_{ij}\frac{\partial u_l}{\partial x_l}\right)\right) + \frac{\partial}{\partial x_j}\left(-\rho\overline{u`_i u`_j}\right) \tag{8}$$

The inlet boundary uses total pressure boundary condition where the value is based on Eq. (1) and Table 1 discussed. The vertical outlet boundary used an open channel mode pressure outlet. For the submerged conditions, the water level of the outlet's open channel is located at the top tip of the turbine. However, the open channel water level is below the turbine for multiphase conditions. The moving mesh cell zone condition is used for the rotating domain based on the desired turbine's rotating speed. The rotation definition must also be stated for the blade boundary.

The coupled pressure-velocity scheme is used in this CFD simulation with the body-force weighted scheme for pressure discretization. The second-order upwind discretization scheme is used for almost all variables calculated in the simulation, including the energy and turbulence-model-based equations. The bounded second-order implicit scheme is used for the time discretization in this simulation with high-order term relaxation. The initiation values are based on the inlet condition with no velocity (zero for u, v, and w). However, for multiphase case simulation, the initial value of the water volume fraction is set as zero. The water volume fraction is designated as one at the nozzle using the patch option to shorten the calculation process. The automatic export and autosave options are turned on for during-calculation activities to obtain the timestep varied calculation results. The timestep size in this simulation is set as 0.0005, which is sufficient for the maximum timestep size based on the Courant number equation in Eq. (9), where the Courant number must not exceed one but better to be closer to one.

$$Cr = \frac{u_{max} \cdot \Delta t}{\Delta x} \tag{9}$$

The CFD simulation in this study used a maximum of 200 iterations per timestep to ensure the accuracy of the calculation. The convergence criteria are tightened to be a maximum of 10^{-6} for the energy equation and 10^{-4} for other equations. For multiphase conditions, this study calculates the turbine works for 1200 timesteps and 700 timesteps for submerged conditions.

This study used the CFD-Post application for the post-processing step of the CFD simulation. The post-processing in this simulation mainly produces the velocity streamline contour. The colouring of the streamline uses various variables: total pressure, turbulence kinetic energy, and the velocity itself. The post-processing in this study is also used to generate some timestep-variable charts, like torque and mass-flow charts, to obtain efficiency.

3. Results and Discussions

The calculation results of all the CFD simulations are reported and discussed in this chapter. Started from the mesh independence test results, discussed in the methodology, and then the step-by-step modification process, followed by a modification summary.

3.1 Mesh Independence Test Results

This study varied three numbers of mesh elements for the mesh independence test: 15,987 elements, 31,979 elements, and 64,020 elements. The simulation was then run for submerged conditions to simplify the independence test process, and then the average turbine torque value at 0 RPM was obtained. After the torque values from all number of elements are received, the prediction by extrapolation of the continuum condition torque value ($f_{h=o}$) then calculated using Eq. (3). The no rotation torque values and GCI values of each number of elements and the extrapolated torque value are briefly displayed in Table 3. The results in Table 3 show that the torque results for the 64k mesh elements have a GCI value of 0.92%. The GCI value is adequate for an independent

mesh size of less than 1%. Moreover, the GCI value is not too small, which means the number of mesh is not too many, so this study doesn't need to interpolate the median value of mesh elements to be used. For the mesh quality, all the generated meshing in this study is maintained to have a skewness valueelow 0.8, which is still classified as a good mesh based on Pulliam and Zingg [17].

Table 3
Mesh independence test results

Elements' number	Refinement ratio	Normalized grid spacing	No rotation torque	Conver-gent order	Extrapolated torque value	GCI
~		0	111.530	-		0
64020		1	109.055	-		0.92%
31979	1.41	1.41	105.585	2.55	111.530	2.22%
15987	1.41	1.9881	97.251	-		5.33%

3.2 The First-step Modification Results

The first modification to the existing CFT in this study is the modification of the turbine blade's profile, especially for the thickness. Besides that, the hub diameter is reduced to ease the water flow through the turbine. Two types of modified blade profiles have the same maximum thickness: A and B. Figure 3(a) shows the first modification results. The graph in Figure 3(a) shows that the modification significantly increases the efficiency. The multiphase condition CFT efficiency increased from 53.2% at 350 RPM to 59.4% at 300 RPM using blade type A and 59.5% at 300 RPM using blade type B, which relatively increased by about 11.8%. On the other hand, the submerged CFT efficiency increased from 51.2% to 58.8% with the type A blade and 59.6% with the type B blade or increased by 16.4% relatively. These results indicate that the B-typed blade profile performs better than the A-type and the existing profiles. Moreover, the submerged CFT efficiency is higher than the multiphase one for the type B blade, indicating improvements in the recirculation and turbulence condition inside the ULH-CFT.

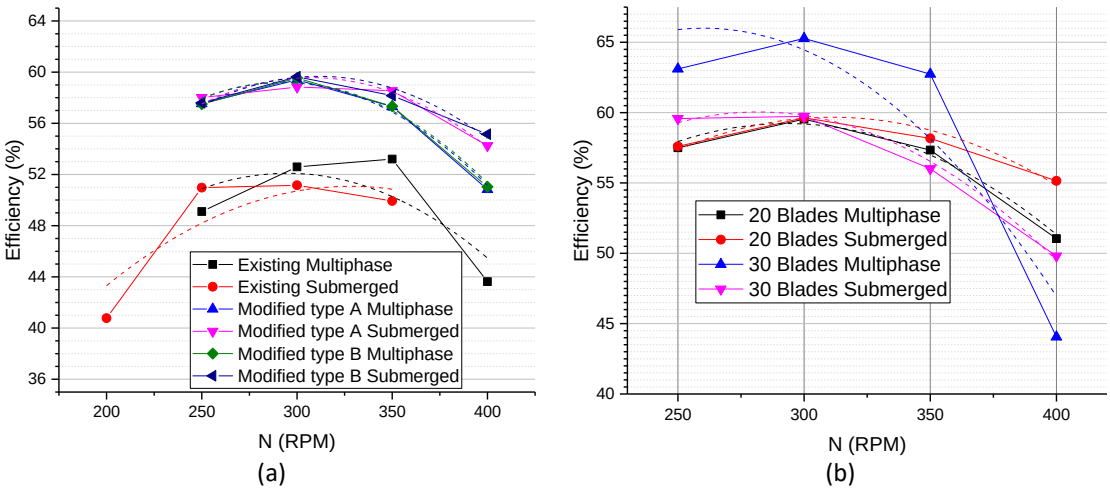

Fig. 3. The step-by-step modification results: (a) first modification, (b) second modification

After obtaining the results, this study investigates the flow patterns inside the ULH-CFT more profoundly. Figure 4 shows the flow patterns inside the ULH-CFT in multiphase and submerged conditions. In multiphase conditions, there is no noticeable recirculation and turbulence in the water flow inside the turbine. It is indicated by all the water flowing inside the turbine being coloured blue or light blue at the turbulence kinetic energy scaled velocity streamline contour. Thus, the water

energy loss during the internal flow is shallow, indicated by the colour of the total pressure mounted water velocity streamlines, and relatively remains the same. However, the improvement only occurred by the effectiveness of the turbine blades at the first and second stages to absorb the water energy. These phenomena indicated by the colour change in the water flow between the blade at the first and second stages in the total pressure velocity streamline for the modified turbine blades are more significant.

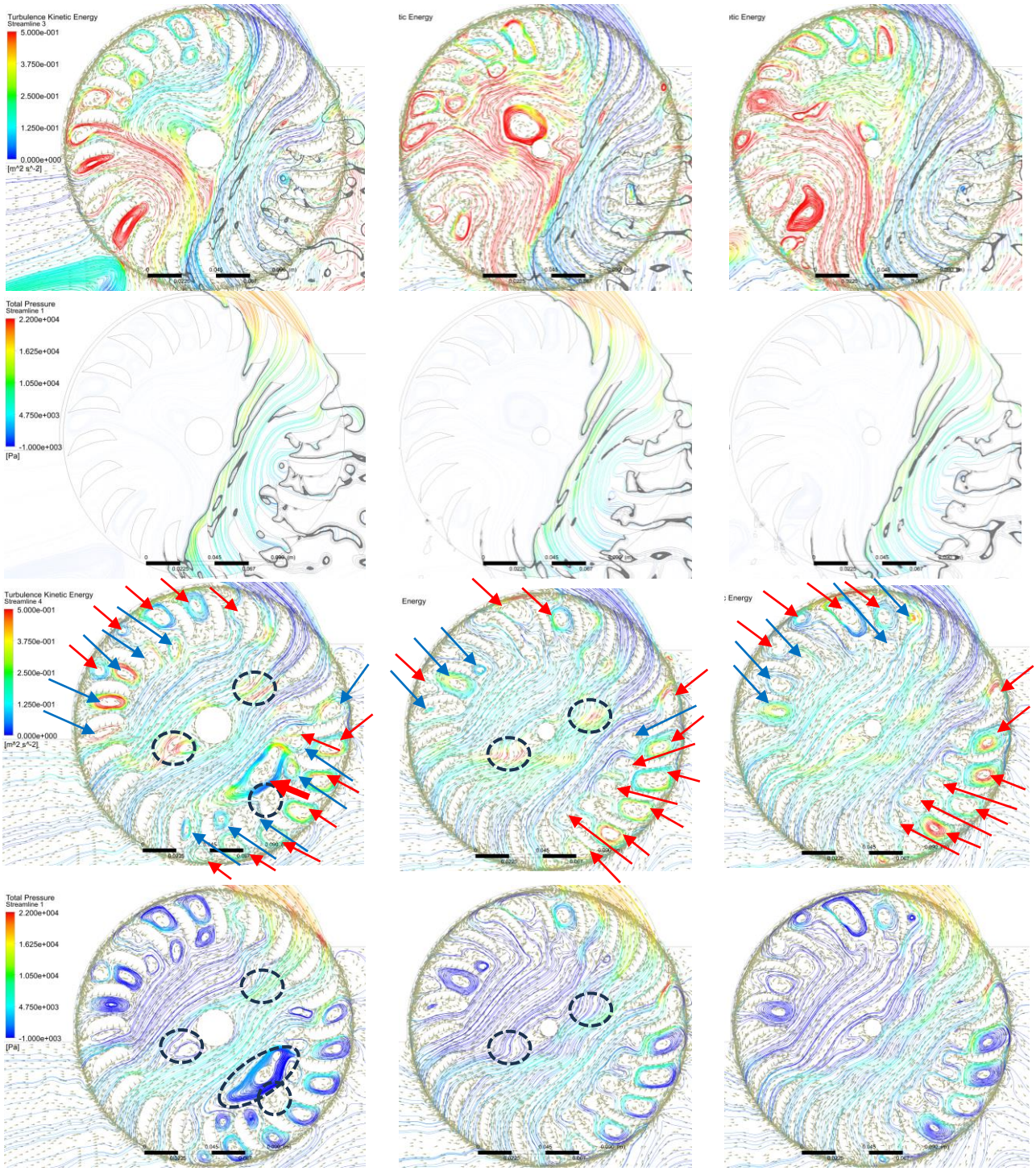

Fig. 4. The flow pattern inside ULH-CFT at first modification

On the other hand, the improvement in the recirculation and turbulence flow occurred more significantly in the submerged CFT conditions. At the existing blade configuration, there are 24 recirculation flows inside the turbine, 54% or 13 in opposite directions with the turbine rotation. However, most of the recirculation flow is located between the blades, which will disappear due to turbine rotation. Only one permanent recirculation flow is located inside the turbine, indicated by a thick arrow in Figure 4, but the direction is opposite the turbine rotation, which will result in negative work to the turbine. Moreover, some flow with high turbulency and a non-moving zone at the back of the turbine blade are also discovered. All of these founded phenomena result in a destructive impact on the turbine performance.

After the blade modification, only 16 recirculation flows are detected at the A-typed blade profile CFT, where only three are rotating along with the turbine rotation. All the recirculation flow is not permanent because it is near the turbine blade. There is no more opposite direction permanent recirculation flow and dead zone. However, some places still have a high turbulency inside the main flow, but less significant than the existing turbine condition. Inside the type A configuration, there are detected 18 recirculation flows, with 5 of them rotating along with the turbine. All the recirculation flows are not perpetual. No more high turbulence kinetic energy flow is detected at the main flow. All these conditions result in the highest turbine work performance.

3.3 The Second-step Modification Results

The results of the second-step modification are briefly displayed in the graph in Figure 3(b). The second modification only changes the number of blades from 20 to 30. The modification only impacts a slight maximum efficiency increase on the submerged CFT scenario from 59.6% to 59.7% but influences a drop in CFT performance at a higher rotational speed. These phenomena indicate that the second modification does not impact better recirculation and turbulence inside the turbine. A tight gap between the blades makes the turbine more likely to rotate the water at a higher RPM.

On the other hand, an impactful improvement occurred on the multiphase ULH-CFT. The maximum efficiency increases from 59.5% to 65.3% or relatively improved by 9.7%. Compared to the existing configuration, the improvement somewhat equals 22.2%. The effectiveness of the water kinetic energy absorption at the denser number of blades mainly causes the improvement. The effectiveness of the energy absorption is indicated by the colour change in the total pressure flow pattern inside Figure 5, which is more significant than the other pattern in Figure 4.

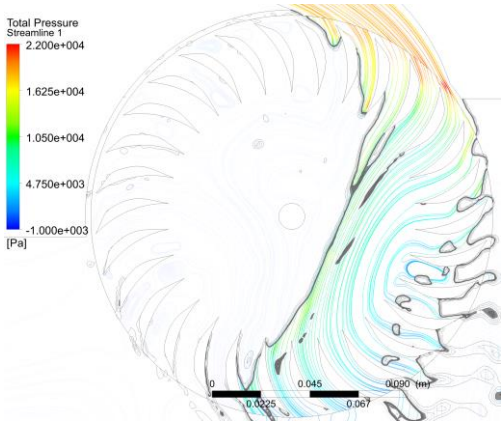

Fig. 5. The second-step modification internal flow pattern

3.4 Comparison to The Prior Studies

The discussions inside subchapters 3.2 and 3.3 show that the modifications during this study increase significantly the ULH-CFT performance. However, another purpose of the modifications conducted in this study is to attain the flow pattern that has a more significant size recirculation flow inside the CFT, as obtained in Elbatran *et al.,* [6] and Picone *et al.,* [7] study, which can be seen in Figure 6(a). In this study, only a tiny recirculation occurred during all the modifications. Thus, other modifications are needed in further studies, especially the nozzle design. However, compared to the experiment results conducted by Sammartano *et al.,* [2] study, the simulation results have relatively similar results, which have an optimum condition together at $^{U}/_{V_T} = \sim 0.56$ (see Figure 6(b)).

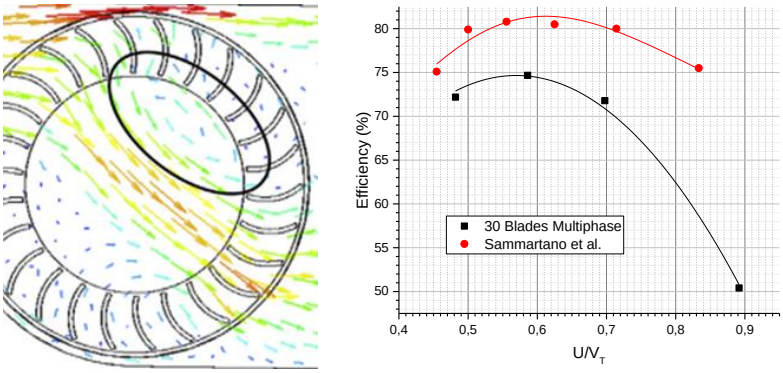

(a) (b)

Fig. 6. The prior study's: (a) Elbatran *et al.,* [6] flow pattern; (b) Sammartano *et al.,* [2] experiment results compared to this simulation

4. Conclusions

The CFT modification conducted in this study can increase this turbine efficiency from 53% to about 66% or relatively increase it by about 24.5% on multiphase conditions. Moreover, at the same time, this turbine performance also improved in submerged conditions during the modification, which increased relatively by about 17.6%. However, the expected recirculation vortex is still tiny, which differs from the studies by Elbatran *et al.,* [6]. Other modifications related to the nozzle design are needed in further studies.

Acknowledgement

This paper's author would like to thank the Research Talent Directorate, National Research and Innovation Agency (BRIN), for supporting this study via Degree By Research (DBR) Program Grants No. B-1832/II.5.4/KU.01.03/4/2023.

References

[1] Mockmore, Charles Arthur, and Fred Merryfield. "The Bank Water Turbine." *Bulletin Series No. 25*. Oregon State College, Corvallis (1949).

[2] Sammartano, Vincenzo, Gabriele Morreale, Marco Sinagra, and Tullio Tucciarelli. "Numerical and experimental investigation of a cross-flow water turbine." *Journal of Hydraulic Research* 54, no. 3 (2016): 321-331. https://doi.org/10.1080/00221686.2016.1147500

[3] Kaniecki, Maciej. "Modernization of the outflow system of cross-flow turbines." *Task Quarterly* 6, no. 4 (2002): 601-608.

[4] Choi, Young-Do, Jea-Ik Lim, You-Taek Kim, and Young-Ho Lee. "Internal flow characteristics of cross-flow hydraulic turbine with the variation of nozzle shape." In *Fluids Engineering Division Summer Meeting*, vol. 42894, pp. 1089-1094. 2007. https://doi.org/10.1115/FEDSM2007-37541

[5] Adanta, Dendy, Budiarso Budiarso, Warjito Warjito, Ahmad Indra Siswantara, and Aji Putro Prakoso. "Performance comparison of NACA 6509 and 6712 on pico hydro type cross-flow turbine by numerical method." *Journal of Advanced Research in Fluid Mechanics and Thermal Sciences* 45, no. 1 (2018): 116-127.

[6] Elbatran, A. H., O. B. Yaakob, Yasser M. Ahmed, and Ahmed S. Shehata. "Numerical and experimental investigations on efficient design and performance of hydrokinetic Banki cross flow turbine for rural areas." *Ocean Engineering* 159 (2018): 437-456. https://doi.org/10.1016/j.oceaneng.2018.04.042

[7] Picone, Calogero, Marco Sinagra, Luana Gurnari, Tullio Tucciarelli, and Pasquale G. F. Filianoti. "A New Cross-Flow Type Turbine for Ultra-Low Head in Streams and Channels." *Water* 15, no. 5 (2023): 973. https://doi.org/10.3390/w15050973

[8] Prabowoputra, Dandun Mahesa, Aditya Rio Prabowo, Yaningsih Indri, Dominicus Danardono Dwi Prija Tjahjana, Fajar Budi Laksono, Adiputra Ristiyanto, and Suryanto Hendri. "Effect of Blade Angle and Number on the Performance of Bánki Hydro-Turbines: Assessment using CFD and FDA Approaches." *Evergreen* 10, no. 1 (2023): 519-530. https://doi.org/10.5109/6782156

[9] Warjito, W., B. Budiarso, K. Celine, and S. B. S. Nasution. "Computational Method for Designing a Nozzle Shape to Improve the Performance of Pico-Hydro Crossflow Turbines." *International Journal of Technology* 12, no. 1 (2021): 139. https://doi.org/10.14716/ijtech.v12i1.4225

[10] Warjito, Warjito, Budiarso Budiarso, Elang Pramudya Wijaya, Kevin Celine, and Sanjaya Baroar Sakti Nasution. "The effect of nozzle-connector angle on cross-flow turbine performance." In *AIP Conference Proceedings*, vol. 2376, no. 1. AIP Publishing, 2021. https://doi.org/10.1063/5.0063477

[11] Adanta, Dendy, Richiditya Hindami, and Ahmad Indra Siswantara. "Blade depth investigation on cross-flow turbine by numerical method." In *2018 4th International Conference on Science and Technology (ICST)*, pp. 1-6. IEEE, 2018. https://doi.org/10.1109/ICSTC.2018.8528291

[12] Adanta, Dendy, Dewi Puspita Sari, Imam Syofii, Aji Putro Prakoso, Muhammad Amsal Ade Saputra, and Ismail Thamrin. "Performance comparison of crossflow turbine configuration upper blade convex and curvature by computational method." *Civil Engineering Journal* 9, no. 1 (2023): 154-165. https://doi.org/10.28991/CEJ-2023-09-01-012

[13] Sammartano, Vincenzo, Costanza Aricò, Armando Carravetta, Oreste Fecarotta, and Tullio Tucciarelli. "Banki-Michell optimal design by computational fluid dynamics testing and hydrodynamic analysis." *Energies* 6, no. 5 (2013): 2362-2385. https://doi.org/10.3390/en6052362

[14] Siswantara, Ahmad Indra, Budiarso Budiarso, Aji Putro Prakoso, Gun Gun R. Gunadi, Warjito Warjito, and Dendy Adanta. "Assessment of turbulence model for cross-flow pico hydro turbine numerical simulation." *CFD Letters* 10, no. 2 (2018): 38-48.

[15] Warjito, Warjito, Budiarso Budiarso, Celine Kevin, Dendy Adanta, and Aji Putro Prakoso. "Computational methods for predicting a pico-hydro crossflow turbine performance." *CFD Letters* 11, no. 12 (2019): 13-20.

[16] Fluent, ANSYS. "Ansys fluent theory guide." *Ansys Inc., USA 15317* (2011): 724-746.

[17] Pulliam, Thomas H., and David W. Zingg. *Fundamental algorithms in computational fluid dynamics*. Vol. 940. New York: Springer, 2014. https://doi.org/10.1007/978-3-319-05053-9